Review

Pore size determination in modified micro- and mesoporous materials. Pitfalls and limitations in gas adsorption data analysis

Johan C. Groen [a,*], Louk A.A. Peffer [a], Javier Pérez-Ramírez [b]

[a] *Applied Catalyst Characterization, DelftChemTech, Delft University of Technology, Julianalaan 136, 2628 BL Delft, The Netherlands*
[b] *Norsk Hydro, Agri Research Centre, Nitric Acid Technology, P.O. Box 2560, N-3907, Porsgrunn, Norway*

Abstract

Physical gas adsorption is extensively used in the characterization of micro- and mesoporous materials and is often considered as a straightforward-to-interpret technique. However, physical phenomena like the tensile strength effect, adsorbate phase transitions, and monolayer formation in combined micro- and mesoporous materials frequently lead to extra contributions in the adsorption isotherm. Models for pore size determination mostly do not account for this, and assignment to real pores leads to improper analysis of adsorption data. In this review, common pitfalls and limitations in the analysis of pore size distributions derived from adsorption isotherms of micro- and mesoporous materials are identified and discussed based on new results and examples reported in the recent literature.
© 2003 Elsevier Science Inc. All rights reserved.

Contents

---

* Corresponding author. Tel.: +31-0-15-278-4371; fax: +31-0-15-278-4452.
  E-mail address: j.c.groen@tnw.tudelft.nl (J.C. Groen).

1. Synthesis and modification of combined micro- and mesoporous materials

Tailoring micro- (pore diameter < 2 nm) and mesoporous (2–50 nm) materials by development of uniform pore size distributions (PSDs) is subject of increasing interest. Uniformly structured mesoporous molecular sieves are synthesized in a way that a tunable pore size in the range of 2–30 nm can be achieved [1–3]. However, the relatively weak acidity and poor hydrothermal properties of these materials have resulted in limited practical applications [4–6]. Traditional microporous molecular sieves, such as zeolites Y, ZSM-5 and beta, have excellent properties related to intrinsic acidity and uniform micropores, with numerous applications in catalysis and separation processes [7–11]. The purely microporous network of zeolites frequently results in intracrystalline diffusion limitations, as a result of the difficult gas transport of reactants to the active sites in the channels or back-diffusion of products [12–15]. Development of more open structures by creating additional porosity, e.g. by combining micro- and mesopores, could lead to significantly improved diffusional properties.

Hierarchically structured porous materials containing both micro- and mesoporosity are generally obtained in two different ways: by newly developed synthesis procedures or by post-synthesis treatments of parent materials. Examples of new synthesis procedures are given by Shan et al. [16,17] and Guo et al. [18], who recently reported the synthesis of bimodal porosity by the incorporation of zeolite beta into a mesoporous matrix of TUD-1 or MCM-41, respectively. Other researchers have shown the successful synthesis of MFI/MCM-41 composites [19,20] and related hierarchical materials [21–24].

Post-synthesis treatments of parent zeolites, which are often used to alter the Si/Al ratio and the corresponding acidic properties, also create a certain extra-porosity due to the presence of defect sites in the zeolite framework upon post-treatment. Consequently, the gas transport characteristics in the material may improve. Well-known treatments include steaming at relatively high temperature or acid leaching, and more recently alkaline treatments. The last method removes mainly Si from the zeolite framework [25–27], while the former ones lead to dealumination [10,28–30]. Dealumination is mainly used to stabilize the zeolite structure or to create Lewis acidity, and the extra-porosity development by steaming is rather limited [13]. The alkaline treatment is more novel and leads to a significant mesopore formation, a lower Si/Al ratio, and small changes in framework acidity. First reports claimed a significantly improved gas transport in alkaline post-treated zeolites leading to enhanced catalytic activities in applications involving acidic sites (cracking of cumene over H-ZSM-5) [12] and metal (iron) species (N_2O decomposition over FeZSM-5) [13].

2. Characterization of pore characteristics of micro- and mesoporous materials

Physical gas adsorption is often the technique of first choice to study the pore characteristics of solid materials and the changes therein upon post-synthesis treatment. The technique accurately de-

termines the amount of gas adsorbed on a solid material, which is a direct measure for the porous properties and structure. In addition, the technique is relatively fast and shows a relatively ease of operation of the equipment. The isotherm obtained from these adsorption measurements provides information on the surface area, pore volume, and PSD [31–33]. Different probe gases including N_2, Ar, and CO_2 are frequently used as adsorptives, depending on the nature of the material (adsorbent) and the information required. N_2 adsorption at 77 K and at sub-atmospheric pressures has remained universally pre-eminent and can be used for routine quality control, as well as for investigation of new materials. If applied over a wide range of relative pressures (p/p_0), N_2 adsorption isotherms provide information on size distributions in the micro-, meso- and macro-porosity range (approximately 0.5–200 nm). The classical pore size model developed by Barret, Joyner and Halenda (BJH) in 1951, which is based on the Kelvin equation and corrected for multilayer adsorption, is most widely used for calculations of the PSD over the mesopore and part of the macropore range [34]. The conventional Horvath–Kawazoe (HK) model for slit-shaped pores (carbons) [35] and the Saito–Foley (SF) model for cylindrical pore geometry (zeolites) [36,37] are mainly applied for micropore size calculations [38–41]. Determination of the micropore size distribution in zeolites is preferentially carried out using Ar adsorption at 87 K (or 77 K). The use of Ar is justified, since the presence of a quadrupolar moment in N_2 can result in enhanced interaction with the heterogeneous surface of the zeolite framework, leading to a more difficult discrimination between zeolites of different pore sizes [42,43]. In addition, N_2 adsorption in micropores occurs at lower p/p_0 values than Ar, the latter being thus more favorable for accurate measurements of smaller micropores [44]. Finally, Ar adsorption at 77 K shows limited application for mesopore size determination, since the coolant temperature is below the bulk triple point. As a consequence, pore condensation vanishes in case the pore diameter exceeds approximately 12 nm [45]. In the case of (activated) carbons, CO_2 is often the preferred adsorptive, since these adsorption mea-

surements are mostly performed at temperatures near ambient, which will enhance diffusion properties in the highly microporous system compared to the low temperatures used in N_2 and Ar adsorption [46,47]. A drawback of CO_2 adsorption at ambient temperature is that in most commonly used equipments, which predominantly operate in the pressure range of vacuum to 1 bar, only a limited range of micropores can be measured, unless high-pressure CO_2 adsorption is used [44, 48]. Other physico-chemical techniques including thermoporo(si)metry, X-ray diffraction and electron microscopy are often used to complement the adsorption results and provide a more detailed picture of the porous and structural aspects of the materials under investigation [49–53].

Due to their relatively simple and well-defined porous structure, the hexagonally ordered M41S materials are very suitable for testing and validation of adsorption theories and models for pore size determination, without complications of non-uniform pore shape and/or pore network effects. The development of these materials has led to the adaptation of existing models and introduction of new models based on non-local density functional theory (NLDFT) and molecular simulations, which were critically evaluated for calculation of PSDs from N_2 and Ar adsorption measurements [52–67]. Although these models clearly prove that the classical BJH model in particular significantly underestimates the real pore size, the classical models (BJH, HK, and SF) are still widely used in the characterization of porous materials. Except for an appropriate description of adsorbate behavior in model mesopores, as discussed in detail elsewhere [52–67], it should also be considered that in practice different physical phenomena during adsorption measurements could significantly affect the adsorption isotherm, leading to *incorrect* assessment of both micro- and mesopore size calculations. In particular, the novel materials representing small mesopores (pore diameter 2–10 nm) and modified materials with combined micro- and mesoporosity are frequently influenced by phenomena as, e.g., the tensile strength effect (TSE) and fluid-to-crystalline like phase transitions of the adsorbed phase.

In this review we will discuss the interpretation of PSDs derived from adsorption isotherms and the

appropriate assignment of different physical phenomena observed in these isotherms. Recently published papers and general reviews on the use of gas adsorption for characterization of porous materials hardly comment on these phenomena [42,68]. As misinterpretations and wrong assignments of adsorption data are strikingly increasing in recent publications, and since they often represent a major conclusion or essential achievement, the impact of this cannot be neglected. This paper should then contribute to prevent misinterpretation of adsorption-derived data. In the first part, the manuscript focuses on the TSE in N_2 adsorption and on fluid-to-crystalline like phase transitions of the adsorbed phase in both N_2 and Ar adsorption, typically observed for MFI-type zeolites. Subsequently, the limitations of micropore size determinations in combined micro- and mesoporous materials are analyzed. The importance and influence of these phenomena will be discussed based on our own experiments and substantiated by multiple examples reported in the literature. A critical appraisal concerning model limitations complements this review.

3. Physical phenomena in gas adsorption

3.1. Tensile strength effect

3.1.1. TSE in adsorption isotherms and impact in pore size determinations

Pore size calculations for determination of the mesopore size distribution can be performed on both the adsorption and desorption branch of the isotherm. In the presence of mesopores, capillary condensation will occur during adsorption and is preceded by a metastable fluid state ("cylindrical meniscus"), while capillary evaporation during desorption occurs via a hemispherical meniscus, separating the vapor and the capillary condensed phase. This will result in hysteresis, since pores of a specific size are filled at higher pressures and emptied at lower pressures.

If the material under investigation is purely mesoporous and contains non-intersecting mesopores of cylindrical geometry and similar size, the N_2 isotherm will be of type IV accompanied by a type H1 hysteresis loop, according to IUPAC classifi-

cation [69]. Both from a historical and thermodynamic point of view, the desorption branch is in these cases often favored to derive mesopore size distributions from the isotherm [53–57]. However, in a more realistic case of a more random distribution of pores and an interconnected pore system, the hysteresis loop will be of type H2 or H3 [69], and the PSD derived from the desorption branch is often much more affected by pore network effects than the adsorption branch [70,71]. This will result in a different behavior of the adsorption and desorption branch of the isotherm, in particular around $p/p_0 = 0.45$ (for N_2 at 77 K), and leads to a forced closure of the hysteresis loop. Fig. 1 represents the N_2 adsorption and desorption isotherms at 77 K of a calcined and alkaline-treated ZSM-5 (for details of the materials see Table 1). The latter shows a pronounced hysteresis at higher p/p_0 as a result of the creation of mesoporosity, which is absent in the calcined sample. The inset in Fig. 1 clearly shows that the forced closure is due to a sudden drop in the volume adsorbed along the desorption branch in the p/p_0 range 0.41–0.48
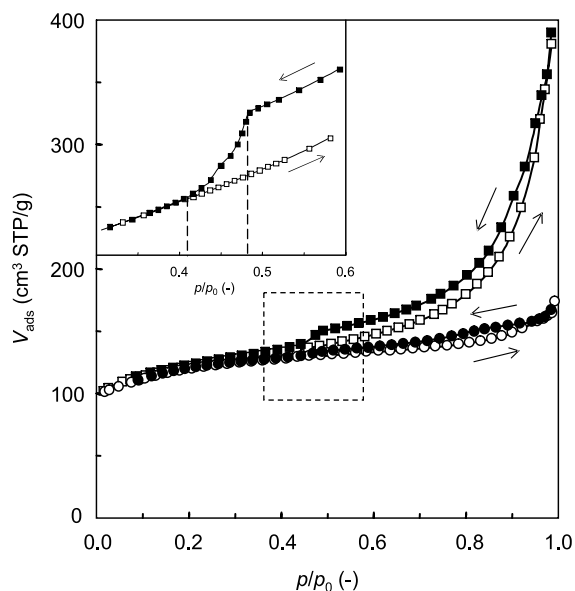
Fig. 1. N_2 adsorption (open symbols) and desorption (solid symbols) isotherms at 77 K of ($\bigcirc$, $\bullet$) calcined and ($\square$, $\blacksquare$) alkaline-treated ZSM-5. Inset figure: a detail of the isotherm in the p/p_0 range 0.3–0.6 (dotted square) emphasizes the TSE at $p/p_0 \sim 0.45$. Conditions of post-treatment as defined in Table 1.

Table 1
Chemical composition of calcined and post-treated ZSM-5 zeolites. The parent zeolite was supplied by Zeolyst: CBV8020, ammonium form, nominal Si/Al = 37.5

Material	Si (wt.%)	Al (wt.%)	Molar Si/Al ratio[d]
ZSM-5 calcined[a]	43	1.1	37
ZSM-5 steamed[b]	43	1.1	37
ZSM-5 alkaline-treated[c]	41	1.6	25

[a] Calcination: air at 823 K for 10 h.
[b] Steam treatment: 30 vol.% H_2O in N_2 at 873 K for 5 h.
[c] Alkaline treatment: 0.2 M NaOH at 353 K for 1 h.
[d] Measured by ICP-OES.

(hereafter denoted as $(p/p_0)_{TSE}$). This phenomenon is often referred to as the Tensile Strength Effect (TSE) [72–74].

In practice, application of the BJH model to the desorption branch of the isotherm will in this case give a completely different result compared to that obtained from the adsorption branch, where the TSE phenomenon is absent. This can lead to misinterpretation of the PSD, as exemplified in Fig. 2 for an alkaline-treated ZSM-5. Not taking into account the TSE phenomenon in the desorption branch PSD would lead to the conclusion that a narrow distribution of pores centered around 4 nm ($d_{TSE} = 3.8$ nm, according to the BJH model) is created upon alkaline post-treatment, while the PSD derived from the adsorption branch evidences that the created mesopores show a broad distribution centered around approximately 10 nm (Fig. 3a). This is in good agreement with the average pore size of approximately 10 nm derived from transmission electron microscopy measurements (Fig. 3b). The peak observed around 4 nm is not reflecting the exact porous properties of the material, but is determined primarily by the nature of the adsorptive.

Nonetheless, in the recent literature the contribution at 3.8 nm is frequently attributed (erroneously) to the presence of real pores. Table 2 summarizes recent examples, where a uniform or narrow mesopore size distribution at approximately 4 nm and bimodal porosity based on "novel synthesis methods" or "post-synthesis treatments" have been claimed. This assignment is in many cases a decisive aspect of the publication, having thus a
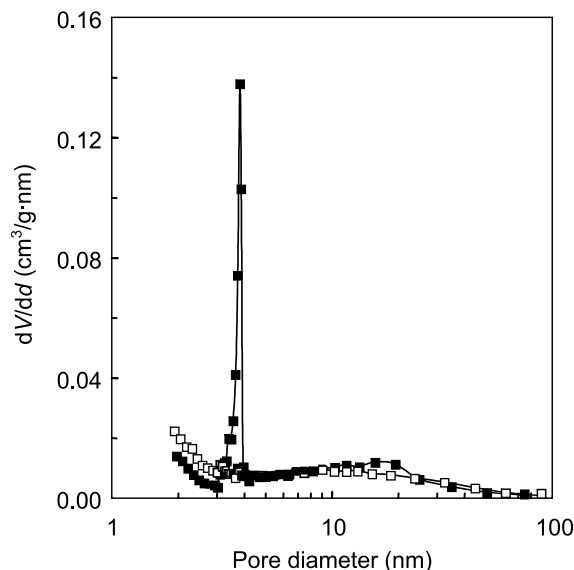
Fig. 2. BJH pore size distribution derived from the (□) adsorption and (■) desorption branch of the isotherm of alkaline-treated ZSM-5. Conditions of post-treatment as defined in Table 1.

more critical impact. Some of these examples were previously discussed by us [27,87]. In many other contributions the TSE phenomenon is also present, but it is not obvious whether the (more cautious) authors fully account for the presence and influence of this contribution on the final result [39,88–91]. Of course, not every narrow PSD at 3.8 nm is necessarily due to the TSE phenomenon. A narrow distribution of real pores at 3.8 nm would show reversibility for both the adsorption and desorption branch [92].

Comparison of the PSD derived from both the adsorption and desorption branch of the isotherm can be used as a diagnostic criterion to evaluate the nature of this phenomenon. The PSD derived from the desorption branch of the isotherm in Fig. 1 clearly shows the artificial pores at approximately 4 nm, while selection of the adsorption branch for pore size calculations indicates the absence of the well-defined distribution of 4 nm pores and shows a much broader distribution around 10 nm (Fig. 3). In case the experimental isotherm shows signs of pore network effects (see Section 3.1.3), the adsorption branch is highly preferred for pore size calculations and is hardly affected by any TSE phenomenon.
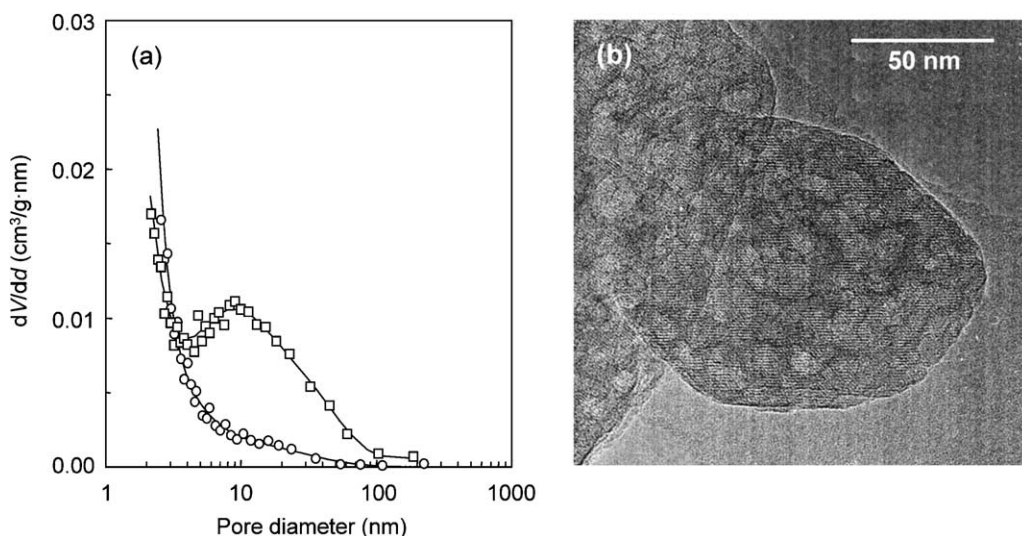
Fig. 3. (a) BJH pore size distribution derived from the adsorption branch of the isotherm of (○) calcined and (□) alkaline-treated ZSM-5. (b) TEM micrograph of alkaline-treated ZSM-5. Conditions of post-treatment as defined in Table 1.

3.1.2. Physical nature of TSE

To better understand the TSE phenomenon, a more detailed analysis of adsorption and desorption processes is required. The filling and emptying of pores of a certain diameter d is historically described by the classical Kelvin equation modified for multi-layer adsorption on the pore wall (t) prior to the onset of condensation or after completing evaporation:

$$(1/2)d = \frac{n\gamma V_L}{RT} + 2t \quad \text{with } n = 1 \text{ for condensation}$$
$$n = 2 \text{ for evaporation}$$
$$(1)$$

where T is the absolute temperature (K) and R is the universal gas constant (J/(mol · K)). γ and V_L represent the surface tension (N/m) and molar volume (cm³/mol) of the liquid adsorbate, respectively. Hysteresis is observed for reasonably large pores ($d > \sim 4$ nm according to the BJH model), and these pores show capillary condensation and evaporation at values for $p/p_0 > 0.45$ (see Fig. 4). However, pores with diameters smaller than 4 nm show no hysteresis and are completely filled and emptied at similar pressures, resulting in a reversible ad- and desorption isotherm. This has been investigated theoretically and experimentally by adsorption on

model systems like MCM-41 and SBA-15 of different pore sizes [30,53,59,66]. Disappearance of the hysteresis in the critical pressure range $(p/p_0)_{TSE}$ seems to be a result of instability of the hemispherical meniscus during desorption in pores with critical diameters approximately 4 nm. This instability of the meniscus is caused by an increased chemical potential of the pore walls, and accordingly an increased tensile strength in the adsorbed phase is observed as the pore size decreases. In case a broad distribution of pores centered around the critical pore diameter is present, both reversible pore filling and capillary condensation will occur. During desorption, larger pores initially will show hysteresis, and upon further pressure decrease the condensed fluid present in the pores with the critical diameter approximately 4 nm ceases to exist and evaporates in the critical $(p/p_0)_{TSE}$ range for N_2 at 77 K, resulting in a forced closure of the hysteresis loop. Subsequently, the emptying of the smaller pores will exhibit reversibility for adsorption and desorption.

The fact that at $(p/p_0)_{TSE}$ a condensed phase is still present actually suggests the presence of somewhat *larger* pores than those corresponding to the emptying pressure (approximately $d_{TSE} = 3.8$ nm). The pores are filled in a relatively broad p/p_0

Table 2
Examples of erroneous assignment of the TSE to real pores at approximately 3.8 nm

System	Peak position in PSD (nm)	Comments in original manuscript	Ref.
ZSM-5 zeolite with uniform 4 nm pores	**4**	Creation of uniform 4 nm pores upon alkaline treatment of ZSM-5 zeolite	[26]
Dealuminated Al-rich zeolites	**3.8**	Narrow peaks suggesting homogeneous pore sized system around 4 nm	[75]
V-MCM-41 and Cr-MCM-41 with hierarchical structure	2.5–2.7, **3.9**	Bimodal PSD in V-MCM-41 and Cr-MCM-41 by simultaneously growing of two types of micelles	[76]
Thermally stable MCM-41 with complementary textural porosity	2.5–2.6, **3.6**	Bimodal framework and textural PSDs suggesting complementary porosity	[77]
Vanadium-doped MCM-41	2–3, **3.8**	V-MCM-41 with bimodal PSD, only the smaller diameter being variable	[78]
Novel aluminosilicate with bimodal mesopore distribution	2.6, **3.8**	Novel aluminosilicate with bimodal PSD and possible application in catalysis and separations	[79]
Micro- and mesoporous titanosilicate catalysts	0.8, **3.6**	Bimodal narrow PSD at 0.8 and 3.6 nm derived from Ar adsorption at 77 K	[80]
TiO_2 photocatalysts by dissolution of titania-silica binary oxides	Micro[a], **3.9**	Mesoporous photocatalyst with uniform pore size of 4 nm	[81]
Novel preparation of high surface area TiO_2 catalyst	**3.5**, ~10	Variable mesopore size around 10 nm and a fixed contribution at 3.5 nm, suggesting bimodal porosity	[82]
Mesoporous zirconium oxide by sol–gel procedure	**3.6**	Sharp mesopore distribution and high surface area	[83]
Pd/Al_2O_3 by sol–gel preparation	**3.6**, 4.5	Narrow PSD centered at 3.6 nm, finally becoming bimodal at 3.6 and 4.5 nm	[84]
Vanadium phosphorous oxide from vanadyl n-butylphosphate	Micro[a], **4.4**	Bimodal distribution with narrow mesopore size at 4.4 nm derived from Dollimore-Heal pore size model	[85]
Preparation of porous SiO_2 from kaolinite	**3.8**	Unimodal pores with average size of 3.8 nm	[86]

[a] The micropore size is not further specified in the manuscript.

range, resulting in a progressive increase in the volume adsorbed on the adsorption branch, while these pores empty in a rather narrow p/p_0 range, causing the mentioned forced closure at $(p/p_0)_{TSE}$. The statement that the presence of *larger* pores is responsible for the TSE phenomenon seems to be in contradiction with the reasoning of Gregg and Sing [74], who oppositely attribute this forced closure to the presence of *smaller* pores. Our hypothesis can be substantiated by N_2 adsorption measurements over MCM-41-like materials presenting reversible condensation and evaporation just below the values of $(p/p_0)_{TSE}$ and d_{TSE} [30,53,59,66,93]. In this case a different condensation and evaporation mechanism has been described for filling and emptying of pores, being an intermediate between micropore filling (supercritical adsorption) for very small pores

($d < 1.4$ nm) and capillary condensation with hysteresis for large pores ($d > 4$ nm). This intermediate process of condensation and evaporation results in *reversibility* for both the adsorption and desorption isotherm. As a consequence pores smaller than d_{TSE} will empty at the same pressure as for condensation, which will be *lower* than the pressure corresponding to the TSE phenomenon. Therefore, it is concluded that these smaller pores can only contribute to the TSE by means of pore network effects.

3.1.3. Pore network effects

The impact of the forced closure of the hysteresis loop at $(p/p_0)_{TSE}$ can become even more pronounced when pore network effects occur and interconnected larger pores have to empty through pores with a smaller diameter, which connect the
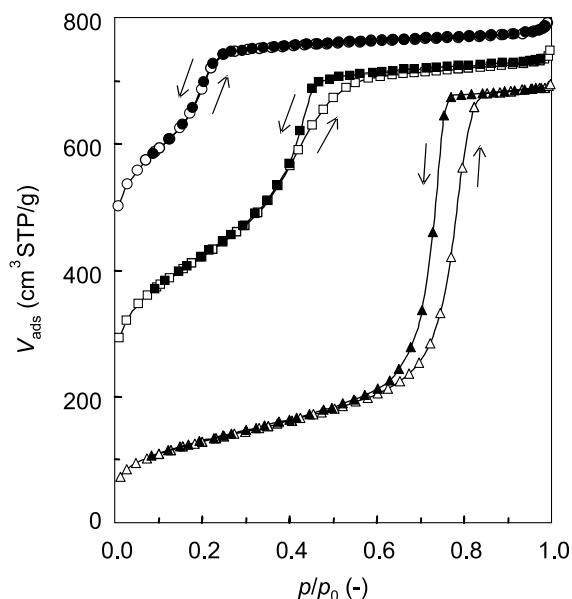
Fig. 4. N_2 adsorption (open symbols) and desorption (solid symbols) isotherms at 77 K of ($\bigcirc$, $\bullet$) MCM-41 (2 nm), ($\square$, $\blacksquare$) MCM-41 (3 nm), and ($\triangle$, $\blacktriangle$) SBA-15 (8 nm).
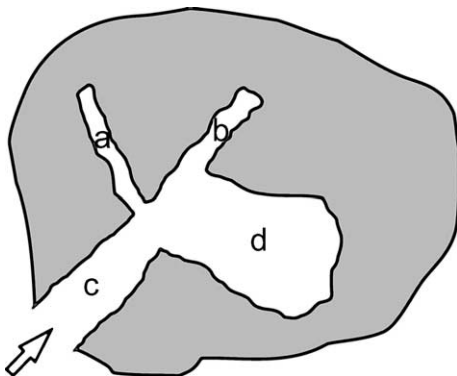
Fig. 5. Pore network effects in adsorption measurements by interconnected (a, b) small, (c) intermediate, and (d) large pores.

larger pores to the outer surface of the particle [71,94]. During desorption, the smaller pores a and b in Fig. 5 will empty at their corresponding pressure, being lower than that needed for emptying of pore c. However, pore d can only empty via pore c and accordingly will empty at lower pressure, even though recent molecular dynamics simulations have shown that pore d can empty through the smaller

pore c while the latter is still filled [95]. This observation differs from the classical idea of pore network and pore blocking effects, although the effect of a delayed evaporation still remains, but will never be observed below the lower limit for hysteresis $(p/p_0)_{TSE}$. Consequently the PSD derived from the desorption branch will generally show a shift to lower pore size than the adsorption branch does, while the latter will provide a more reliable picture of the actual pore system. Van Der Voort et al. [23] recently reported on the development of plugged hexagonal templated silicas containing both open and encapsulated mesopores. N_2 adsorption and desorption experiments on these materials result in a step-wise desorption isotherm, suggesting bimodal porosity, while the adsorption branch shows only one step representing the size of both the open and blocked mesopores (Fig. 6). The step-wise desorption isotherm is due to the fact that the encapsulated mesopores empty at lower pressure than the open pores of similar size.

3.1.4. Nature of the adsorptive and temperature dependency

The parameter $(p/p_0)_{TSE}$ is influenced by the nature of the adsorptive and the analysis temperature, as shown in Fig. 7. The adsorption and desorption isotherms (at 77 K) of NaOH-treated ZSM-5 using different adsorptives (N_2, Ar, Kr) clearly evidence the shift in the TSE, while the pore characteristics of the adsorbent obviously remain unchanged. The desorption branch of the isotherm shows a forced closure at $p/p_0 = 0.42$, 0.25, and 0.03 in the case of N_2, Ar and Kr, respectively. These results are in accordance with literature [30,59,74,96]. The temperature dependency of hysteresis has been discussed in detail elsewhere [55,96,97].

3.2. Fluid-to-crystalline phase transitions in MFI zeolites

The microporous properties of zeolites are frequently studied by adsorption of N_2 and Ar, in particular for materials belonging to the MFI framework type (ZSM-5 and silicalite) [98]. In general, adsorption on zeolites results in a type I isotherm [69], indicative of microporosity and a limited mesoporosity. On these materials the *t*-plot
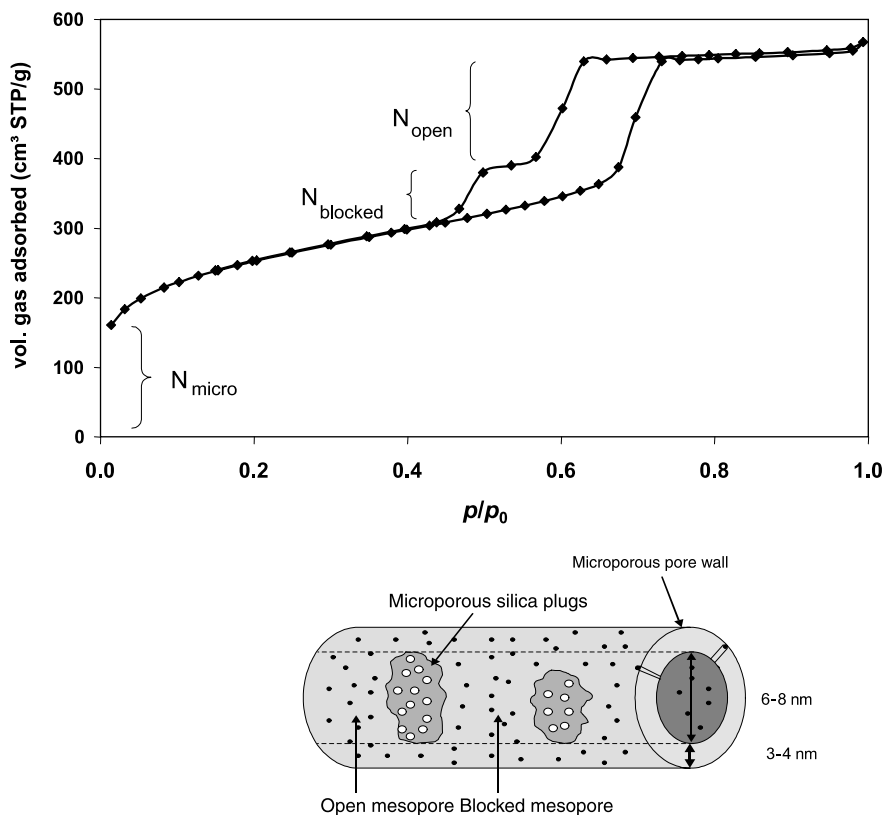
Fig. 6. N$_2$ 77 K isotherm of a typical plugged hexagonal templated silica material [24] (reproduced by permission of The Royal Society of Chemistry).

[99] or α_s-plot [100] can be used to acquire information on the micropore volume. However, when detailed information on the micropore size and its distribution is needed, *high-resolution low-pressure* adsorption is required to study the filling of the micropores [42,43,101–103]. Most commonly used adsorption equipment starts measurements at p/p_0 around 0.01 and higher, where the micropores are already filled to a large extent and no information can be derived on their size distribution. In low-pressure adsorption measurements p/p_0 values are monitored starting from 10^{-6} or 10^{-7} up to 1. A detailed description on high-resolution low-pressure equipment is given by Borghard et al. [104]. In addition to the given pressure transducers of 1000 mmHg (133 kPa) and 10 mmHg (1.33 kPa), an optional 1 mmHg (0.13 kPa) pressure transducer is essential in order to achieve an optimal resolution in the very-low-pressure range. In the case of zeo-lites, Ar is often preferred for acquisition of low-pressure data, since the presence of the quadrupolar moment in N$_2$ results in enhanced interaction with the zeolite framework [42,43]. Adsorption measurements with both adsorptives are influenced by peculiar characteristics of the MFI framework, leading to a step-wise isotherm (Fig. 8), with extra steps at $p/p_0 = 10^{-3}$ (Ar) and $p/p_0 = 0.1$–0.2 (N$_2$). The fact that this additional step is observed at higher pressures in N$_2$ adsorption ($p/p_0 = 0.1$–0.2) is related to the weaker interactions of Ar with the adsorbent, where the step is observed at lower pressure ($p/p_0 = 10^{-3}$) [102].

This step-wise behavior can be explained by a *fluid-to-crystalline* like phase transition of the adsorbed phase in the micropores, and does not indicate any real porosity. The explanation that a phase transition is responsible for this sub-step behavior was supported by volumetric
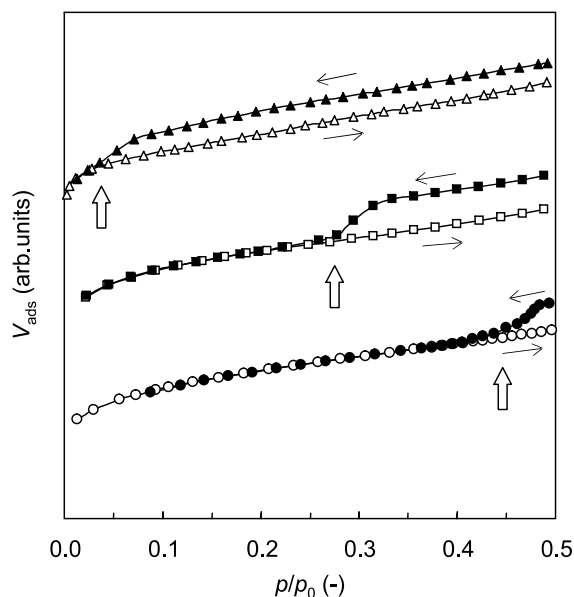
Fig. 7. Adsorption (open symbols) and desorption (solid symbols) isotherms at 77 K of alkaline-treated ZSM-5 using different adsorptives: ($\bigcirc$, $\bullet$) N_2, ($\square$, $\blacksquare$) Ar, and ($\triangle$, $\blacktriangle$) Kr. Conditions of post-treatment as defined in Table 1.
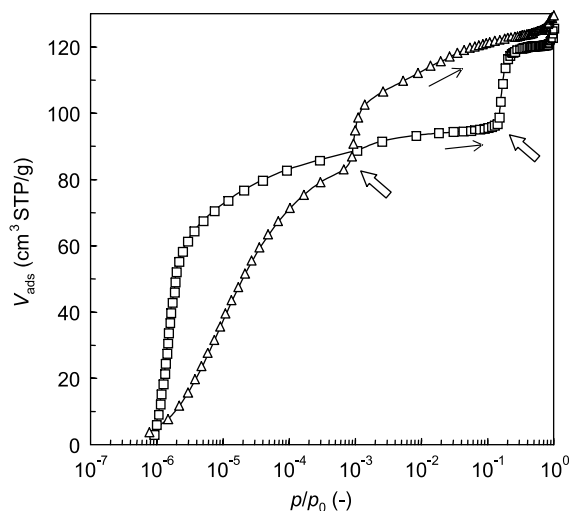
Fig. 8. High-resolution ($\square$) N_2 and ($\triangle$) Ar adsorption isotherms of silicalite-1, measured at 77 K and 87 K, respectively.

microcalorimetry and neutron diffraction techniques [105,106]. The density of the molecules in the adsorbed phase increases from around 23 (fluid phase) to 30 (crystalline phase) molecules per unit cell (assuming 1.04×10^{20} unit cells per gram of zeolite) [103]. The phase transition seems to be dependent on the energetic properties of the micropore surface. An energetically homogeneous surface will result in a well-pronounced sub-step in a narrow p/p_0 range, while a more heterogeneous surface will show a more diffuse step, covering a broader p/p_0 range. In the case of MFI zeolites, this largely depends on the *framework* Si/Al ratio (Si/Al)$_{framework}$. Materials with very high Si/Al ratios (Si/Al > 100, e.g. the purely siliceous end member silicalite-1) present an energetically rather homogeneous surface, while increasing the Al content (towards ZSM-5) induces energetic heterogeneity [102].

Application of the SF model to the Ar adsorption isotherm in Fig. 8 would lead to a bimodal PSD, showing the expected 0.55 nm peak, corresponding to the straight and zig-zag channels in the MFI structure, and an extra contribution around 0.8 nm, related to non-existing pores, by assignment of the sub-step to real pores rather than to the phase transition (inset Fig. 9b) [102]. Application of classical mesopore size models (e.g. BJH) to the N_2 isotherm would result in an additional contribution in the PSD just below 2 nm, again representing non-existing pores (inset Fig. 9a).

Several publications [25,102,107–110] have reported the sub-step behavior in adsorption measurements, and the explanations given for this phenomenon are not always consistent. Some authors [108] suggested a smaller micropore volume in silicalite-1 compared to ZSM-5, while others [109] claim that a monoclinic to orthorhombic transition of the adsorbent framework [111] is the cause of this behavior. However, this slight change in coordination upon framework transition cannot fully account for this step-wise behavior [105].

Marked changes in the shape of the isotherm are observed upon steam treatment of calcined H-ZSM-5, as shown in Fig. 9. Steam treatment induces the extraction of tetrahedral Al to extra-framework positions [13,112], increasing the (Si/Al)$_{framework}$ ratio, but not changing the overall Si/Al ratio in the sample (see Table 1). It is believed that Al extraction is followed by Si migration to stabilize the framework, finally leading to an energetically more homogeneous pore surface. This correlates
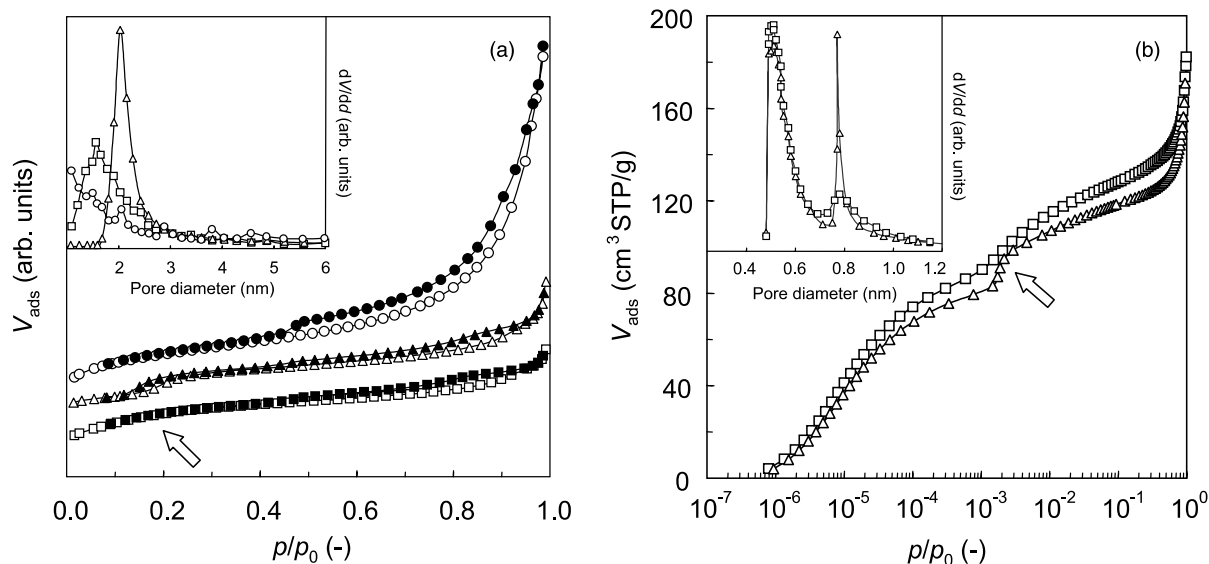
Fig. 9. (a) N_2 adsorption (open symbols) and desorption (solid symbols) isotherms at 77 K of ($\square$, $\blacksquare$) calcined, ($\triangle$, $\blacktriangle$) steamed, and ($\bigcirc$, $\bullet$) alkaline-treated ZSM-5. Isotherms have been rescaled to separate the curves of the different materials in the phase transition range. (b) High-resolution Ar adsorption isotherms at 87 K of ($\square$) calcined and ($\triangle$) steamed ZSM-5. Inset figures: PSD derived from the adsorption branch according to the BJH and SF model, respectively. Conditions of post-treatment as defined in Table 1.

with the sub-step in the N_2 and Ar adsorption isotherm, which is accordingly more pronounced in the steamed material than in the calcined sample. This result suggests the presence of the generated extra-framework Al species at the external surface of the zeolite crystals, creating a more (energetically) uniform pore wall. The slightly lower uptake found for the steamed material is caused by the presence of extra-framework species, probably blocking micropores. The inset in Fig. 9b shows the bimodal PSD according to the SF model applied to the Ar adsorption isotherm, with a more pronounced contribution around 0.8 nm for the steamed material, by assignment of the phase transition to real pores. A distinct contribution representing non-existing pores around 2 nm is derived from the N_2 isotherm of the steamed sample according to the BJH adsorption PSD (inset in Fig. 9a).

Upon alkaline treatment of calcined ZSM-5, both the overall Si/Al and the (Si/Al)$_{framework}$ ratio are significantly decreased (Table 1), and contrarily a less pronounced contribution around 2 nm would be expected. Application of the BJH model to the N_2 adsorption isotherms of the calcined and alkaline-treated sample (inset Fig. 9a) indeed shows a

minor contribution around 2 nm for the alkaline-treated sample compared to the calcined material. However, Suzuki and Okuhara [25] concluded the formation of uniform pores of 2 nm upon alkaline treatment of ZSM-5 zeolite, which is in contradiction with our expectations and observations, although the assignment seems to be related to the adsorbate phase transition phenomenon.

Recent developments on conventional models for micropore size calculations have, in particular, implemented a more appropriate description of the interaction parameters between adsorptives and adsorbents with various pore geometries [113–115]. However, the effect of fluid-to-crystalline like phase transitions on the micropore size distribution has hardly been taken into account. This task is complicated, and even the use of more sophisticated models developed by NLDFT have been unsuccessful so far. These models will also include an extra peak in the PSD. Fig. 10 indeed shows, apart from the expected contribution of ZSM-5 at 0.56 nm, an extra peak (non-existing pores) around 0.9 nm in the PSD derived from the Ar adsorption isotherm on silicalite-1 (Fig. 8) by application of a recently developed NLDFT model describing argon
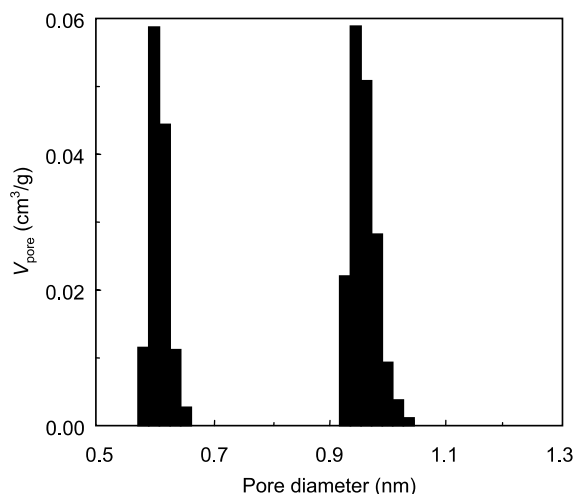
Fig. 10. NLDFT micropore size distribution derived from the Ar adsorption isotherm of silicalite-1 at 87 K (see Fig. 8).

adsorption on zeolite–SiO$_2$ composites [116]. Despite the fact that this model was designed for Ar adsorption on zeolite–SiO$_2$ composite materials, a similar result is obtained as for the PSD calculated by the classical SF model. The phenomenon is limited to MFI zeolites, due to the specific framework properties of these materials, not being a critical aspect for other framework types. However, one should be aware that MFI is, among other

zeolites as faujasite and A-type structures, widely applied in catalytic and separation processes.

3.3. Monolayer formation in combined micro- and mesoporous materials

Proper analysis and interpretation of high-resolution low-pressure adsorption data of materials with combined micro- and mesoporosity is also of practical relevance. A high degree of mesoporosity, leading to a high mesopore surface area, can significantly affect the low-pressure part (micropore range) of the isotherm and thus the micropore size calculations by conventional HK and SF models. Fig. 11a shows the low-pressure Ar adsorption isotherms of a purely mesoporous MCM-41 ($S_{BET} = 1100$ m^2 g^{-1}) and TUD-1 ($S_{BET} = 450$ m^2 g^{-1}) [16], with pore diameters of approximately 2 nm and 10 nm, respectively. The isotherms show the typical steps in the higher p/p_0 range, corresponding to capillary condensation in the mesopores. Though these materials are purely mesoporous, the PSD derived from these adsorption isotherms by application of the SF model (Fig. 11b) shows a broad diffuse peak within the micropore range, suggesting microporosity around 1 nm. The contribution in MCM-41 seems to be larger than in the lower surface area TUD-1 material. If a physical mixture of
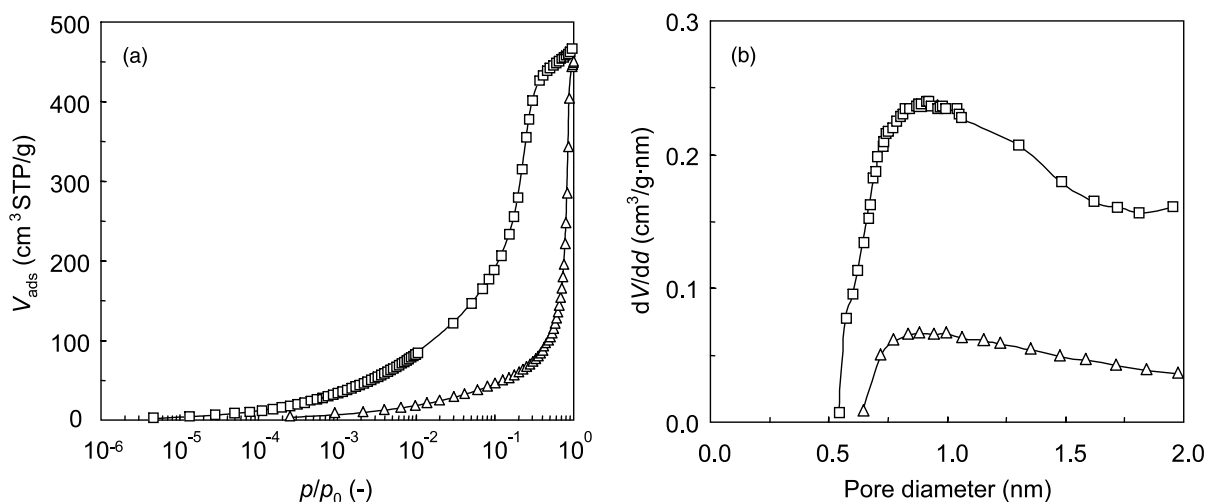
Fig. 11. (a) High-resolution Ar adsorption isotherms at 87 K and (b) derived SF micropore size distribution of (□) mesoporous MCM-41 (2 nm) and (△) TUD-1 (10 nm).
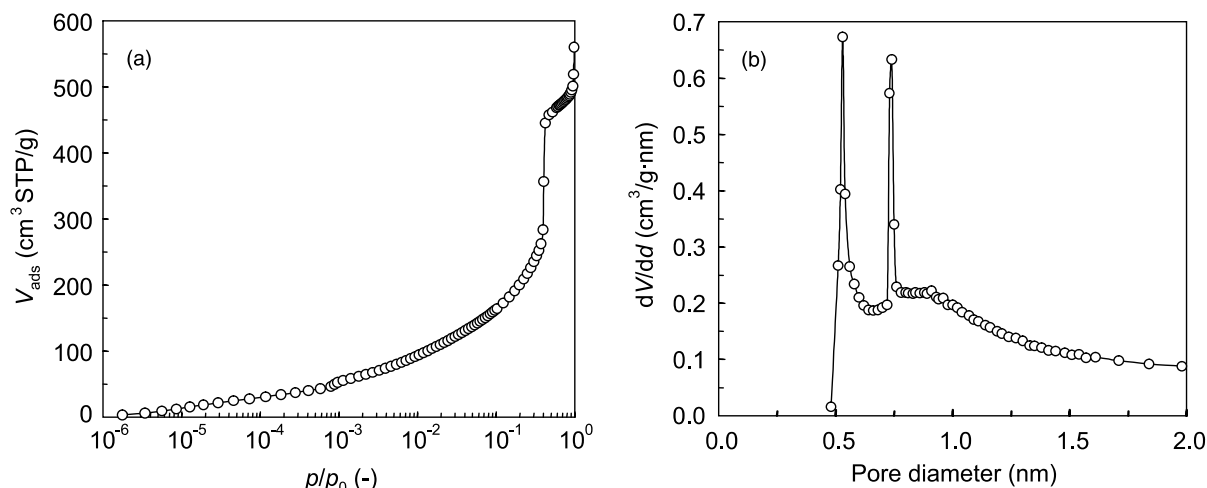
Fig. 12. (a) High-resolution Ar adsorption isotherms at 87 K and (b) derived SF micropore size distribution of a physical mixture of MCM-41 (4 nm) and ZSM-5.

35 wt.% ZSM-5 and MCM-41 is analyzed, different contributions can be identified in the isotherms and micropore size distributions, as presented in Fig. 12. The first contribution corresponds to filling of the characteristic 0.55 nm micropores of ZSM-5, while the second peak (phase transition, see Section 3.2), is observed on a broad and diffuse contribution due to the presence of the mesoporous MCM-41.

This diffuse contribution at ∼1 nm is the result of monolayer formation in mesopores [42], which already occurs at relatively low pressures and is both dependent on the mesopore size and mesopore surface area. The contribution will shift to somewhat lower pressure in smaller mesopores and consequently shows a peak in the micropore size distribution at smaller pore diameter, while a larger mesopore surface area will enhance the significance of this contribution (Fig. 11b).

Inadequate analysis of this phenomenon can lead to conclusions like a broadened micropore size distribution, where a shoulder in the HK micropore size distribution due to the presence of additional mesoporosity has been interpreted as microporosity [117]. Other authors [85] have abusively claimed the presence of microporosity, derived from a diffuse contribution in the HK PSD, which is clearly a result of mesoporosity. The distribution obtained was very similar to that shown in Fig. 11b. In the same publication the authors showed that *t*-plot extra-

polation passes through the origin, a conclusive diagnosis for the absence of microporosity.

Application of a reference isotherm of a purely mesoporous material (representing a similar mesopore size and a comparable mesopore surface area) can be used to correct for this mesoporosity contribution. This approach was successfully applied in the synthesis and characterization of different zeolite beta-TUD-1 composites [17]. Initially a broad distribution of micropores is measured in the composites; especially those materials with a low loading of beta show a much broader PSD than in pure beta used to prepare the composites (see Fig. 13). However, after correction for the mesopore contribution a similar micropore size distribution was found, where both the shape of the micropore size distribution and the micropore volume very well correlate with the loading used in the preparation of the composites. Obviously, this method is only applicable when appropriate reference materials are available.

Application of the comparative *t*-plot and α_s method can also be a relevant approach to obtain information on the micropore volume. Again, this requires suitable reference data. Furthermore, these models do not provide information on the micropore size.

Revisited HK and SF models do not account for the effect of mesoporosity on micropore size
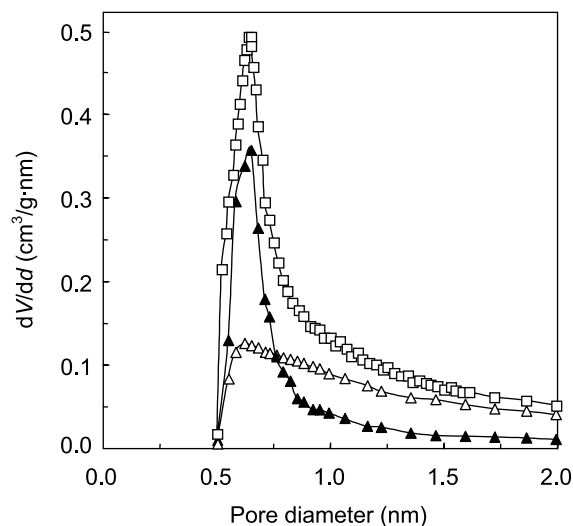
Fig. 13. SF micropore size distribution derived from Ar adsorption at 87 K on a 40% beta-TUD-1 composite: (□) directly derived from the isotherm of the mixed composite, (△) contribution of TUD-1, and (▲) contribution of beta.

Fig. 14. NLDFT pore size distribution of a 40 wt.% beta-TUD-1 composite covering the micro- and mesopore size range. Inset figure: a detail of the micropore size range.

distributions [113–115]. NLDFT models should be able to improve calculation of the micropore size distribution considerably. However, most of the models developed so far are based on *ideal* cylindrical pore geometry and particularly applicable in the mesopore range. Consequently, limitations in the appropriate description of geometrical and energetic effects of the pore and pore wall will often lead to a discrepancy between the experimental and calculated isotherm, especially in the lower p/p_0 range of the isotherm [57]. In this lower pressure range, where interactions between adsorbate and adsorbent are most important, a step-wise behavior is often observed in the calculated isotherm, leading to *apparent* (micro)porosity. In these cases also NLDFT cannot quantitatively describe the microporosity present in the composite material under investigation. Application of the recently developed NLDFT model describing argon adsorption on zeolite–SiO_2 composites [116] shows the bimodal PSD in the micro- and mesopore range derived from the Ar low-pressure isotherm at 87 K of a 40 wt.% zeolite beta-TUD-1 composite (Fig. 14). Both contributions correspond to the characteristics of the individual materials. The PSD in the micropore range (inset in Fig. 14) hardly shows any influence

from the mesoporosity of TUD-1, and no significant contribution is observed for pore diameters >1 nm. Furthermore, the calculated micropore volume is, as expected, based on the 40 wt.% loading. In this particular case the model adequately describes both the micro- and mesopore size range for the composite material.

4. Conclusions and perspectives

Physical gas adsorption is often considered as a conventional, relatively fast and straightforward-to-interpret technique. However, phenomena like the TSE, adsorbate phase transitions, and monolayer formation in combined micro- and mesoporous materials often lead to misapprehension due to the assignment of these contributions to real pores. The increasing development of more sophisticated porous materials for catalytic and separation processes, which in particular are susceptible to these phenomena, thus requires a more fundamental understanding and critical interpretation of the adsorption data. A general recommendation for proper interpretation of adsorption data, especially for pore size calculations, is that the shape of the isotherm (both adsorption and desorption branch)

including the hysteresis loop is taken into consideration.

Conventional models (BJH, HK, SF) are very useful to analyze adsorption data, but only apply to a given part of the isotherm. Consequently, these models can only partially deal with adsorption in the more sophisticated materials and should not be used following a "*press button*" approach in commercial software. A solid background for correct interpretation is obviously required. Development of (NL)DFT models, accompanied by molecular simulations and molecular dynamics, has led to a better understanding of adsorption processes in well-ordered systems compared to the more conventional models. However, the perception that the models developed so far can adequately cover the whole p/p_0 range of the isotherm for pore size calculations, thus avoiding the use of separate models to calculate micro- and mesopore size distributions, has shown limited practical application. Major limitations of these models are the non-allowance for network effects and a poor description of the geometrical and energetic effects of the pore and pore wall [118]. The development of both robust models *and* well-defined reference materials would surely improve the accuracy and reliability of calculated PSDs for micro- and mesoporous materials.

Acknowledgement

References

[1] J.S. Beck, J.C. Vartuli, W.J. Roth, M.E. Leonowicz, C.T. Kresge, K.B. Schmitt, C.T.-W. Chu, D.H. Olsen, E.W. Shepard, S.B. McCullen, J.B. Higgins, J.L. Schlenker, J. Am. Chem. Soc. 114 (1992) 10834.

[2] C.T. Kresge, M.E. Leonowicz, W.J. Roth, J.C. Vartuli, J.S. Beck, Nature 359 (1992) 710.

[3] D. Zhao, J. Feng, Q. Huo, N. Melosh, G. Frederickson, H. Glenn, B.F. Chmelka, G.D. Stucky, Science 279 (1998) 548.

[4] A. Corma, V. Fornes, M.T. Navarro, J. Pérez-Pariente, J. Catal. 148 (1994) 569.

[5] M.E. Davis, Nature 364 (1993) 391.

[6] A. Sayari, Chem. Mater. 8 (1996) 1840.

[7] A.E.W. Beers, T.A. Nijhuis, F. Kapteijn, J.A. Moulijn, Micropor. Mesopor. Mater. 48 (2001) 279.

[8] M.A. den Hollander, M. Wissink, M. Makkee, J.A. Moulijn, Appl. Catal. A: Gen. 223 (2002) 85.

[9] F. Collignon, G. Poncelet, J. Catal. 202 (2001) 68.

[10] J. Pérez-Ramírez, F. Kapteijn, G. Mul, J.A. Moulijn, Chem. Commun. (2001) 693.

[11] J. Pérez-Ramírez, F. Kapteijn, G. Mul, J.A. Moulijn, J. Catal. 208 (2002) 211.

[12] M. Ogura, S.Y. Shinomiya, J. Tateno, Y. Nara, M. Nomura, E. Kikuchi, M. Matsukata, Appl. Catal. A: Gen. 219 (2001) 33.

[13] J. Pérez-Ramírez, F. Kapteijn, J.C. Groen, A. Doménech, G. Mul, J.A. Moulijn, J. Catal. 214 (2003) 33.

[14] A. Corma, A. Martinez, V. Martinez-Soria, J. Catal. 200 (2001) 259.

[15] X. Zhao, G.Q. Lu, G.J. Millar, Ind. Eng. Chem. Res. 35 (1996) 2075.

[16] Z. Shan, J.C. Jansen, L. Marchese, Th. Maschmeyer, Micropor. Mesopor. Mater. 48 (2001) 181.

[17] Z. Shan, W. Zhou, J.C. Jansen, C.Y. Yeh, J.H. Koegler, Th. Maschmeyer, in: A. Sayari, M. Jaroniec (Eds.), Nanoporous Materials III, Studies in Surface Science and Catalysis, vol. 141, Elsevier, Amsterdam, 2002, p. 635.

[18] W. Guo, L. Huang, P. Deng, Z. Xue, Q. Li, Micropor. Mesopor. Mater. 44–45 (2001) 427.

[19] A. Karlsson, M. Stöcker, R. Schmidt, Micropor. Mesopor. Mater. 27 (1999) 181.

[20] L. Huang, W. Guo, P. Deng, Z. Xue, Q. Li, J. Phys. Chem. B 104 (2000) 2817.

[21] Y. Liu, W.Z. Zhang, T.J. Pinnavaia, J. Am. Chem. Soc. 122 (2000) 8791.

[22] Y. Liu, W.Z. Zhang, T.J. Pinnavaia, Angew. Chem. Int. Ed. 40 (2001) 1255.

[23] P. Van Der Voort, M. Benjelloun, E.F. Vansant, J. Phys. Chem. B 106 (2002) 9027.

[24] P. Van Der Voort, P.I. Ravikovitch, K.P. De Jong, A.V. Neimark, A.H. Janssen, M. Benjelloun, E. Van Bavel, P. Cool, B.M. Weckhuysen, E.F. Vansant, Chem. Commun. (2002) 1010.

[25] T. Suzuki, T. Okuhara, Micropor. Mesopor. Mater. 43 (2001) 83.

[26] M. Ogura, S.-H. Shinomiya, J. Tateno, Y. Nara, E. Kikuchi, M. Matsukata, Chem. Lett. (2000) 882.

[27] J.C. Groen, J. Pérez-Ramírez, L.A.A. Peffer, Chem. Lett. (2002) 94.

[28] J. Scherzer, ACS Symp. Ser. 248 (1984) 157.

[29] M. Müller, G. Harvey, R. Prins, Micropor. Mesopor. Mater. 34 (2000) 135.

[30] P.L. Llewellyn, Y. Grillet, F. Schüth, H. Reichert, K.K. Unger, Micropor. Mater. 3 (1994) 345.

[31] S.J. Gregg, K.S.W. Sing, Adsorption Surface Area and Porosity, second ed., Academic Press, London, 1982, p. 303.

[32] F. Rouquerol, J. Rouquerol, K.S.W. Sing, Adsorption by Powders and Porous Solids, Academic Press, London, 1999, p. 467.

[33] S. Lowell, J.E. Shields, Powder, Surface Area and Porosity, third ed., Chapman and Hall, London, 1991, p. 250.

[34] E.P. Barret, L.G. Joyner, P.H. Halenda, J. Am. Chem. Soc. 73 (1951) 373.

[35] G. Horvath, K. Kawazoe, J. Chem. Eng. Jap. 16 (1983) 470.

[36] A. Saito, H.C. Foley, Micropor. Mater. 3 (1995) 531.

[37] A. Saito, H.C. Foley, AIChE J. 37 (1991) 429.

[38] K. Okada, A. Shimai, Y. Shigeo, A. Yasumori, Clay Sci. 11 (1999) 73.

[39] H. Wang, Z. Wang, L. Huang, A. Mitra, B. Holmberg, Y. Yan, J. Mater. Chem. 11 (2001) 2307.

[40] J. Pérez-Ramírez, J.M. García-Cortés, F. Kapteijn, G. Mul, J.A. Moulijn, C. Salinas-Martínez de Lecea, Appl. Catal. B: Environ. 29 (2001) 285.

[41] A. Gil, M.A. Vicente, L.M. Gandia, Micropor. Mesopor. Mater. 34 (2000) 115.

[42] S. Storck, H. Bretinger, W.F. Maier, Appl. Catal. A: Gen. 174 (1998) 137.

[43] A.F. Venero, J.N. Chiou, Mater. Res. Soc. Proc. 111 (1988) 235.

[44] P.I. Ravikovitch, A. Vishnyakov, R. Russo, A.V. Neimark, Langmuir 16 (2000) 2311.

[45] M. Thommes, R. Köhn, M. Fröba, Appl. Surf. Sci. 196 (2002) 239.

[46] F. Rouquerol, J. Rouquerol, K.S.W. Sing, Adsorption by Powders and Porous Solids, Academic Press, London, 1999, p. 255.

[47] F. Rodríguez-Reinoso, M. Molina-Sabio, Adv. Colloid Interface Sci. 76–77 (1998) 271.

[48] D. Cazorla-Amorós, J. Alcañiz-Monge, M.A. de la Casa-Lillo, A. Linares-Solano, Langmuir 14 (1998) 4589.

[49] R. Denoyel, M.T.J. Keene, P.L. Llewellyn, J. Rouquerol, J. Therm. Anal. Calorim. 56 (1999) 261.

[50] K.R. Kloetstra, H.W. Zandbergen, M.A. van Koten, H. van Bekkum, Catal. Lett. 33 (1995) 145.

[51] A.H. Janssen, A.J. Koster, K.P. de Jong, Angew. Chem. Int. Ed. 40 (2001) 1102.

[52] M. Kruk, M. Jaroniec, A. Sayari, Langmuir 13 (1997) 6267.

[53] J.C. Groen, M.C. Doorn, L.A.A. Peffer, in: D.D. Do (Ed.), Adsorption Science and Technology, World Scientific, Singapore, 2000, p. 229.

[54] P.I. Ravikovitch, S.C. O'Domhnaill, A.V. Neimark, F. Schüth, K.K. Unger, Langmuir 11 (1995) 4765.

[55] A.V. Neimark, P.I. Ravikovitch, A. Vishnyakov, Phys. Rev. E 62 (2000) R1493.

[56] A.V. Neimark, P.I. Ravikovitch, in: K.K. Unger, G. Kreysa, J.P. Baselt (Eds.), Characterization of Porous Solids V, Studies in Surface Science and Catalysis, vol. 128, Elsevier, Amsterdam, 2000, p. 51.

[57] P.I. Ravikovitch, A.V. Neimark, J. Phys. Chem. B 105 (2001) 6817.

[58] P.I. Ravikovitch, D. Wei, W.T. Chueh, W.T. Haller, A.V. Neimark, J. Phys. Chem. B 101 (1997) 3671.

[59] A.V. Neimark, P.I. Ravikovitch, M. Grun, F. Schüth, K.K. Unger, J. Colloid Interface Sci. 207 (1998) 159.

[60] P.I. Ravikovitch, A.V. Neimark, Colloid Surf. A 187 (2001) 11.

[61] P.I. Ravikovitch, A.V. Neimark, Micropor. Mesopor. Mater. 44 (2001) 697.

[62] M. Jaroniec, M. Kruk, J.P. Olivier, S. Koch, in: K.K. Unger, G. Kreysa, J.P. Baselt (Eds.), Characterization of Porous Solids V, Studies in Surface Science and Catalysis, vol. 128, Elsevier, Amsterdam, 2000, p. 71.

[63] M.W. Maddox, J.P. Olivier, K.E. Gubbins, Langmuir 13 (1997) 1737.

[64] W.A. Steele, M.J. Bojan, Adv. Colloid Interface Sci. 76–77 (1998) 153.

[65] C.G. Sonwane, S.K. Bathia, Chem. Engng. Sci. 53 (1998) 3143.

[66] C.G. Sonwane, S.K. Bathia, J. Phys. Chem. B 104 (2000) 9099.

[67] W.W. Lukens, P. Schmidt-Winkel, D. Zhao, J. Feng, G.D. Stucky, Langmuir 15 (1999) 5403.

[68] K.S.W. Sing, Colloid Surf. A 187–188 (2001) 3.

[69] K.S.W. Sing, D.H. Everett, R.A.W. Haul, L. Moscou, R.A. Pierotti, J. Rouquerol, T. Siemieniewska, Pure Appl. Chem. 57 (1985) 603.

[70] D.H. Everett, in: S.J. Gregg, K.S.W. Sing, H.F. Stoeckli (Eds.), Characterization of Porous Solids, Soc. Chem. Ind, London, 1979, p. 229.

[71] N.A. Seaton, Chem. Engng. Sci. 46 (1991) 1895.

[72] O. Kadlec, M.M. Dubinin, J. Colloid Interface Sci. 31 (1969) 479.

[73] C.V.G. Burgess, D.H. Everett, J. Colloid Interface Sci. 33 (1970) 611.

[74] S.J. Gregg, K.S.W. Sing, Adsorption Surface Area and Porosity, second ed., Academic Press, London, 1982, p. 154.

[75] R. Le Van Mao, G. Denes, N.T.C. Vo, J.A. Lavigne, S.T. Le, Mat. Res. Soc. Proc. 371 (1995) 123.

[76] Z.Y. Yuan, J.Z. Wang, Z.L. Zhang, T.H. Chen, H.X. Li, Micropor. Mesopor. Mater. 43 (2001) 227.

[77] H. Chen, Y. Wang, Ceram. Int. 28 (2002) 541.

[78] P.C. Schulz, M.A. Morini, M. Palomeque, J.E. Puig, Colloid Polym. Sci. 280 (2002) 322.

[79] Z.Y. Yuan, J.Z. Wang, H.X. Li, Chinese Chem. Lett. 8 (1997) 927.

[80] A. Keshavaraja, V. Ramaswamy, H.S. Soni, A.V. Ramsawamy, P. Ratnasamy, J. Catal. 157 (1995) 501.

[81] Q. Zhang, L. Gao, S. Zheng, Chem. Lett. (2001) 1124.

[82] G. Colón, M.C. Hidalgo, J.A. Navío, Catal. Today 76 (2002) 91.

[83] V.I. Pârvulescu, H. Bonneman, V. Pârvulescu, U. Endruschat, A. Rufinska, Ch.W. Lehmann, B. Tescha, G. Poncelet, Appl. Catal. A: Gen. 214 (2001) 273.

[84] C.K. Lambert, R.D. Gonzalez, J. Mater. Sci. 34 (1999) 3109.

[85] Y. Kamiya, E. Nishikawa, A. Satsuma, M. Yoshimune, T. Okuhara, Micropor. Mesopor. Mater. 54 (2002) 277.

[86] J. Temuujin, G. Burmaa, J. Amgalan, K. Okada, T. Jadambaa, K.J.D. Mackenzie, J. Porous Mater. 8 (2001) 233.

[87] J.C. Groen, L.A.A. Peffer, J. Pérez-Ramírez, Micropor. Mesopor. Mater. 51 (2002) 75.

[88] K. Kang, H. Rhee, in: A. Galarneau, F. Di Renzo, F. Fajula, J. Vedrine (Eds.), Zeolites and Mesoporous Materials at the Dawn of the 21st Century, Studies in Surface Science and Catalysis, vol. 135, Elsevier, Amsterdam, 2001, p. 4678.

[89] N.R.B. Coleman, G.S. Attard, Micropor. Mesopor. Mater. 44–45 (2001) 73.

[90] K.C. Song, S.E. Pratsinis, J. Mater. Res. 15 (2000) 2322.

[91] L. Huang, Z. Wang, H. Wang, J. Sun, Q. Li, D. Zhao, Y. Yan, Micropor. Mesopor. Mater. 48 (2001) 73.

[92] S. Jun, R. Ryoo, J. Catal. 195 (2000) 237.

[93] R. Schmidt, M. Stöcker, E. Hansen, D. Akporiaye, O.H. Ellestadt, Micropor. Mater. 3 (1995) 443.

[94] M.W. Maddox, C.M. Lastoskie, N. Quirke, K.E. Gubbins, in: M.D. LeVan (Ed.), Fundamentals in Adsorption, Kluwer, Boston, 1996, p. 571.

[95] L. Sarkisov, P.A. Monson, Langmuir 17 (2001) 7600.

[96] K. Morishige, H. Fujii, M. Uga, D. Kinukawa, Langmuir 13 (1997) 3494.

[97] K. Morishige, M. Shikimi, J. Chem. Phys. 108 (1998) 7821.

[98] C.h. Baerlocher, W.M. Meier, D.H. Olson, Atlas of Zeolite Framework Types, fifth ed., Elsevier, Amsterdam, 2001, p. 184.

[99] B.C. Lippens, J.H. de Boer, J. Catal. 4 (1965) 319.

[100] K.S.W. Sing, in: D.H. Everett, R.H. Ottewill (Eds.), Surface Area Determination, Butterworths, London, 1970, p. 25.

[101] P.E. Hathaway, M.E. Davis, Catal. Lett. 5 (1990) 333.

[102] A. Saito, H.C. Foley, Micropor. Mater. 3 (1995) 543.

[103] W.S. Borghard, P.T. Teischman, E.W. Sheppard, J. Catal. 139 (1993) 19.

[104] W.S. Borghard, E.W. Sheppard, H.J. Schoennagel, Rev. Sci. Instrum. 62 (1991) 2801.

[105] P.L. Llewellyn, J.-P. Coulomb, Y. Grillet, J. Patarin, G. Andre, J. Rouquerol, Langmuir 9 (1993) 1846.

[106] P.L. Llewellyn, J.-P. Coulomb, Y. Grillet, J. Patarin, H. Lauter, H. Reichert, J. Rouquerol, Langmuir 9 (1993) 1852.

[107] H. Reichert, U. Müller, K.K. Unger, Y. Grillet, F. Rouquerol, J. Rouquerol, J.P. Coulomb, in: F. Rodriguez-Reinoso, J. Rouquerol, K.S.W. Sing, K.K. Unger (Eds.), Characterization of Porous Solids II, Elsevier, Amsterdam, 1991, p. 535.

[108] R. Lai, G.R. Gavalas, Ind. Eng. Chem. Res. 37 (1998) 4275.

[109] G.L. Marra, G. Tozzla, G. Leofanti, M. Padovan, G. Petrini, F. Genoni, B. Venturelli, A. Zecchina, S. Bordiga, G. Richiardi, in: J. Weitkamp, H.G. Karge, H. Pfeifer, W. Hölderich (Eds.), Zeolites and Related Microporous Materials: State of the Art, Studies in Surface Science and Catalysis, vol. 84, Elsevier, Amsterdam, 1994, p. 559.

[110] Y.S. Ko, W.S. Ahn, Micropor. Mesopor. Mater. 30 (1999) 283.

[111] G. Engelhardt, D. Michel, High-Resolution Solid-State NMR of Silicates and Zeolites, Wiley, UK, 1987, p. 312.

[112] J. Pérez-Ramírez, G. Mul, F. Kapteijn, J.A. Moulijn, A.R. Overweg, A. Doménech, A. Ribera, I.W.C.E. Arends, J. Catal. 207 (2000) 113.

[113] S.U. Rege, R.T. Yang, AIChE J. 46 (2000) 734.

[114] R.J. Dombrowski, C.M. Lastoskie, D.R. Hyduke, Colloid Surf. A 187–188 (2001) 23.

[115] E.A. Ustinov, D.D. Do, Langmuir 18 (2002) 4637.

[116] M. Thommes, Quantachrome's Particle Technology News 4 (2) (2001).

[117] T. Yamada, K. Johkan, T. Okuhara, Micropor. Mesopor. Mater. 26 (1998) 109.

[118] A. Sayari, M. Kruk, M. Jaroniec, Catal. Lett. 49 (1997) 147.